Data-driven methodological approach for modeling rainfall-induced infiltration effects on combined sewer overflow in urban catchments

Violeta Montoya-Coronado, Damien Tedoldi, Hélène Castebrunet, Pascal Molle, Gislain Lipeme Kouyi

Journal of Hydrology 632 (2024) 130834

Contents lists available at ScienceDirect

Journal of Hydrology

journal homepage: www.elsevier.com/locate/jhydrol

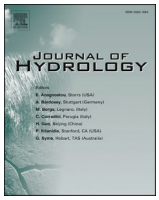

Research papers

Data-driven methodological approach for modeling rainfall-induced infiltration effects on combined sewer overflow in urban catchments

V.A. Montoya-Coronado [a,*], D. Tedoldi [a], H. Castebrunet [b], P. Molle [c], G. Lipeme Kouyi [a]

[a] INSA Lyon, DEEP, UR7429, 69621 Villeurbanne, France
[b] Université Grenoble Alpes, IGE, F-38000, Grenoble, France
[c] INRAE, Research Unit REVERSAAL, Lyon, France

ARTICLE INFO

This manuscript was handled by Corrado Corradini, Editor-in-Chief, with the assistance of Wei Hu, Associate Editor

Keywords:
Combined sewer overflow
Parsimonious urban hydrology model
Rainfall-induced infiltration
Stormwater management
Sustainable Urbain Drainage Systems

ABSTRACT

Combined sewer system deterioration poses significant challenges, especially as it leads to substantial volumes of Permanent Infiltration Inflow (PII) and Rain-Induced Infiltration (RII) to percolate into sewer pipes. This infiltration increases the risk of Combined Sewer Overflow (CSO) events and reduces the treatment plant's efficiency by diluting raw effluent. To effectively decrease CSO volumes, it is crucial to identify the various flow components and their contribution to overflow volumes. In this study, a data-driven hydrological model was developed, conceptualizing the surface hydrological processes as well as the interactions between soil water and the sewer system, based on long-term monitoring. Four flow components at the outlet of the catchment were identified and characterized: wastewater, surface runoff, PII, and RII. The model was applied and evaluated using monitored data from the Ecully catchment in France. The model demonstrated its suitability in replicating the observed hydrograph and estimating CSO volumes. Two sewer system scenarios were proposed, investigating the effect of partial and complete reduction of PII and RII on CSO volumes. The results showed a reduction of the annual CSO volume by 5 % to 7.5 %, and 12 % to 17 %, in the first and second scenario, respectively. To compare the performance of these scenarios with stormwater management strategies, two other scenarios were considered where source control measures allowed infiltration of the first 5 and 10 mm of rainfall. The results demonstrated that these measures could, respectively, reduce CSO volumes by 13 % to 48 % and completely eliminate CSO for half of the events. This study highlights the limitations of relying solely on PII and RII strategies to eliminate CSO events and emphasizes the necessity of considering stormwater management strategies.

1. Introduction

The traditional drainage system with end-of-pipe solutions has been proven ineffective to face the increasing urban sprawl (Marsalek and Chocat, 2002) due to the numerous well-known negative effects caused by the hydrological changes of the catchment area and the hydraulic dysfunctions of the sewer system (Fletcher et al., 2013; Zhou, 2014). Furthermore, its low capacity to cope with upcoming challenges such as climate change and the need to provide long-term sustainability (Zhou et al., 2019) have led to question the relevance of this system as the dominant model for urban drainage.

In addition to usual hydraulic failures, inflow of water into the sewer pipes can occur continuously through cracks, joints, or defects in the pipes, or due to leakage from drinking water systems (Kidmose et al., 2015) leading to what is usually referred to as Permanent Infiltration Inflow (PII). Additionally, during and/or after a storm event, water can percolate into the buried sewer pipes by infiltrating into the soil and then into the sewer pipes, which is commonly known as Rainfall-Induced Infiltration (RII). As numerous European countries have an asset renewal rate below 1 % (The European Federation of National Water Services, 2017), sewer failures are inevitable and wastewater treatment efficiency decreases (Ellis and Bertrand-Krajewski, 2010; Schulz et al., 2005; Staufer et al., 2012). In addition to problems related to the dilution of the effluents, the increasing volume due to PII and RII in the sewer system leads to an increased risk of Combined Sewer Overflows (CSO) characterized by discharges of untreated wastewater into receiving waters (Dirckx et al., 2019).

As the volume of permanent infiltration inflow and rain-induced infiltration depends on the local tightness of the pipes, the interaction with the buried sewer system is still difficult to estimate without a

* Corresponding author at: INSA Lyon, DEEP, UR7429, 69621 Villeurbanne, France.
E-mail address: violeta-alexandra.montoya-coronado@insa-lyon.fr (V.A. Montoya-Coronado).

https://doi.org/10.1016/j.jhydrol.2024.130834
Received 25 October 2023; Received in revised form 21 December 2023; Accepted 17 January 2024
Available online 3 February 2024

measurement campaign. Their estimation could be carried out on different time scales, from daily to hourly, using flow and/or water quality monitoring methods (Bareš et al., 2009; Kracht and Gujer, 2005; Weiß et al., 2002). Moreover, such approaches are only able to describe the current state of the sewer system and do not allow for scenario exploration. For this reason, *in situ* measurements are often used to feed and build models. Those models are then used to understand the key processes of the study system and explore different scenarios for urban planning, among whose objectives is the reduction of CSO events and volumes.

Recent research has focused on the modelling of source control measures and the impact of their dissemination in the urban catchment. Golden and Hoghooghi (2018) consider it as an emerging science, indeed, current hydrological-hydraulic models often lack the holistic approach to consider the interactions between surface, subsurface and sewer systems. This oversight is understandable considering the complexity to conceptualize these interactions which are influenced by numerous natural and anthropogenic processes that interact with each other across different spatio-temporal scales (Salvadore et al., 2015). The difficulty increases when attempting to conceptualize the hydraulic processes of CSO structures widespread in the sewer system. Further scientific challenge is assessing the contribution of permanent and rain-induced infiltration on CSO. These issues are probably interrelated, as several authors raised questions about the potential increase of these components if stormwater source control measures are disseminated in the catchment area (Bonneau et al., 2017; Pophillat et al., 2021).

In previous studies, different approaches have been applied to identify and quantify infiltration inflow components prior to their integration in a model, such as: (i) assessing infiltration inflow based on wastewater and stormwater conductivity at the event scale (Wang et al., 2019; Zhang et al., 2018); (ii) statistical methods, derived from observed infiltration data, correlating Infiltration Inflow to the site/sewer characteristics such as material, size, shape, soil type, and water table (Liu et al., 2021), or the dynamics to the sewer water composition (Sowby and Jones, 2022); (iii) mechanistic models describing the locations where water may percolate into the buried sewer pipes (Zhang and Parolari, 2022); (iv) coupling different modeling tools; for example, MODFLOW (Harbaugh, 2005) is used to simulate variations in the water table, thus providing data to feed hydrological and hydraulic models (Fryd et al., 2013; Roldin et al., 2012); and (v) simplified representation of Infiltration Inflow through constant flow injections in the sewer system (Andrés-Doménech et al., 2010; Jean et al., 2021). Although most existing models focus on event-based simulations, regulatory standards for discharges from combined sewer systems generally apply on an annual scale (Botturi et al., 2021). This raises the question of whether it is worthwhile turning to models based on annual continuous simulation rather than event-based simulations with simple methods, especially when limited data is available.

To our knowledge, while significant modelling efforts have been devoted to the impact of stormwater management strategies on CSO mitigation (Bonneau et al., 2023; Jean et al., 2022; Mahaut and Andrieu, 2019; Torres et al., 2022), limited studies account for the surface and the subsurface processes and the sewer system at the urban catchment scale, allowing to investigate the contribution of permanent and rain-induced infiltration to CSO. Schulz et al. (2005) and Dirckx et al. (2019) highlighted the need for a direct method that can distinguish between stormwater and the other components of the hydrograph arriving at the CSO structure to determine whether the primary contributor is permanent and rain-induced infiltration or other sewer system components. So as to investigate this matter, the present study combines data analysis with hydrological and hydraulic modelling. More specifically, the originality lies in examining the contribution of permanent and rain-induced infiltration on CSO using continuous flow data, and proposing a parsimonious model adaptable to the available data. The model

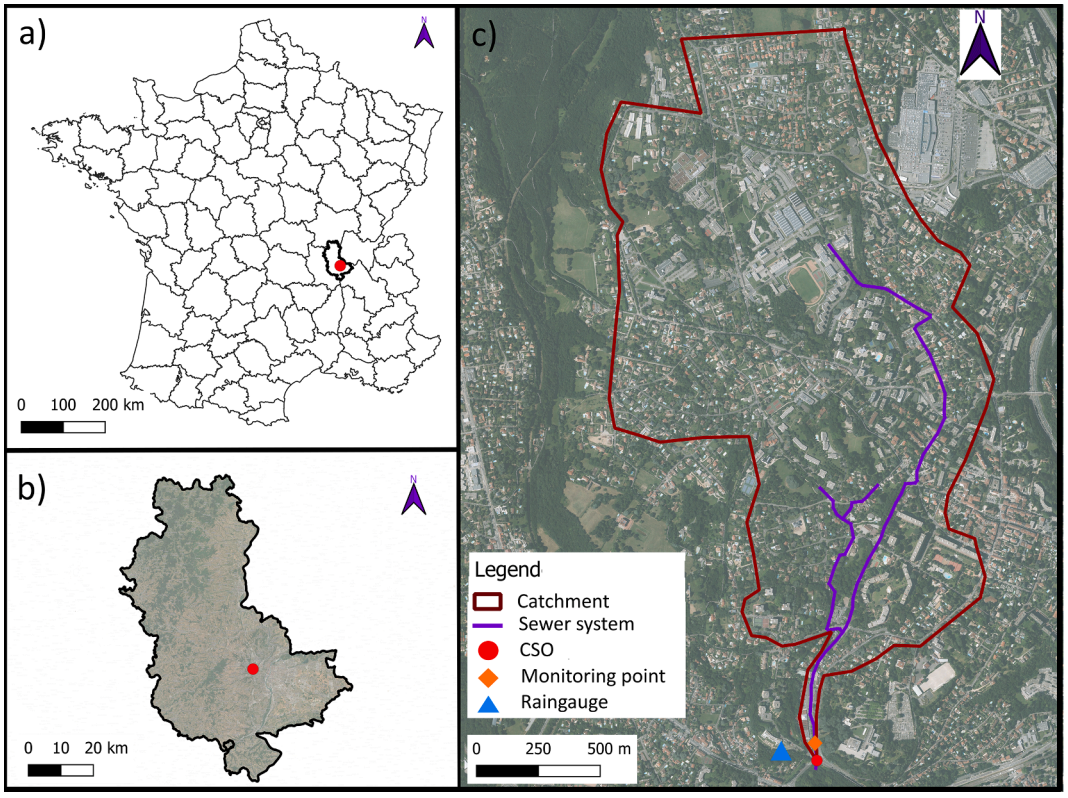

Fig. 1. Ecully catchment location a) within France, b) within the Rhone department and c) within Ecully city. The catchment is delineated by a brown boundary. The combined sewer system main pipes are represented by lines, the Combined Sewer Overflow structure (CSOs) is marked by a red point, the monitoring point (i.e., water level and velocity) is marked by a diamond and the rain gauge is marked by a triangle. (For interpretation of the references to colour in this figure legend, the reader is referred to the web version of this article.)

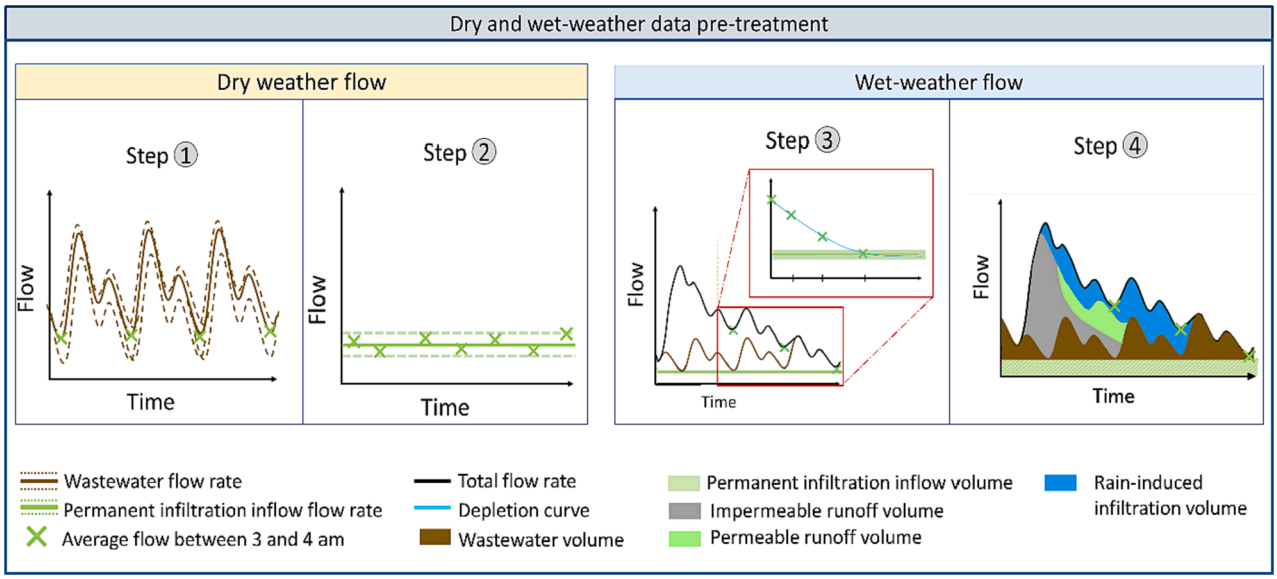

Fig. 2. Diagram of the methodology for dry and wet-weather data pre-treatment. Step 1 and Step 2 illustrate the dry weather flow components: wastewater and permanent infiltration inflow. Step 3 and 4 illustrate wet-weather flow components: impervious surface runoff, permeable surface runoff and rain-induced infiltration.

describes the key processes coupling surface and infiltration inflow components at the urban catchment scale. The aim was to identify and quantify the different flow components in a combined sewer system and thus to develop a non-demanding but reliable modelling framework enabling the assessment of water management strategies to reduce CSO volumes. A particular attention was paid to the evaluation of the model's ability to provide event-based water balance and dynamics at the outlet of the catchment and thus, estimate the CSO volumes and frequency.

The model was developed and evaluated in the context of a French case study. The paper presents the following applications of the model:

- Assessing the significance of the permanent infiltration inflow and rain-induced infiltration by identifying their potential contribution to CSO volumes.
- Investigating if the model can assist, as part of a planning management tool, for CSO volume reduction planning management by decomposing the dynamic profile of all hydrological components characterizing the outlet of urban catchment.
- Evaluating impacts of permanent infiltration inflow and rain-induced infiltration reduction scenarios in reducing CSO volume, CSO events frequency and duration; comparing the performance to global disconnection scenarios.

2. Material and methods

2.1. Concepts and terminology

In this study, the focus is on a combined sewer system designed to collect wastewater during dry weather conditions and stormwater throughout rain events. Such systems are equipped with hydraulic structures designed to prevent flooding of untreated water in case of high flow rates, ensuring a rapid discharge of a fraction of this water to the receiving environment (e.g., rivers and lakes). These hydraulic structures are commonly referred to as "Combined Sewer Overflow structures" (CSOs). The outflow rate from CSOs is typically designated as the "CSO rate". Integrating the CSO rate over time at the scale of a rainfall event yields the discharged volume, subsequently referred to as the "CSO volume".

The system of interest in this study, which we aim to model, includes the CSOs and its catchment, i.e., the surface that contributes to wastewater production, stormwater runoff, and possibly PII and RII, all of which converge in the pipe located immediately upstream of the CSOs. The total flow is then subdivided into a conserved flow (towards the Wastewater Treatment Plant) and possibly a CSO rate discharged into the receiving environment (river, lake). The latter is not considered in this study.

Sewage pipes might not always be watertight, leading to drainage of water that infiltrates from the surrounding ground. Such drained water is known as "infiltration inflow" (I/I). In this study, we further divide I/I into two distinct components: Permanent Infiltration Inflow (PII), and Rain-Induced Infiltration (RII). The former corresponds to the constant base flow observed in the sewer regardless of the time of day; this component may be due to water constantly infiltrating through the buried pipes, possibly from groundwater or a drinking water leak. The latter is the rainwater that infiltrates through the soil and reaches the sewer due to its porosity; it is thus observable only during or after a rainfall event. Our study encompasses the surface and the sewer system, which only interacts with the environment through what enters the pipes. Subsurface flows, which may constitute additional inputs to the river, are not taken into account since the system's downstream boundary is the CSOs.

2.2. Description of study area and monitoring data

The residential catchment of Ecully is located in the northwest of Lyon in the Rhone department, France (Fig. 1). The drainage area of 245 ha is partially urbanized with approx. 18,000 inhabitants in 2007 and 42 % of impervious surface. The catchment is drained by a combined sewerage system with an average slope of 2 %. The longest water path in the sewer system is 1.8 km. In case of a storm event, the excess flow is discharged to the river through a CSOs referred as "Ecully Valvert" and located at the outlet of the Ecully catchment (Fig. 1).

The CSOs was continuously monitored by a long-term monitoring program in urban hydrology called OTHU (https://othu.graie.org). The site was equipped with water level, flow velocity and rainfall sensors, among other devices not relevant to this study. Reliable monitoring data are available for the period 2007–2010.

Water levels were measured in duplicates by piezometer probes (NIVUS-OCM Pro and Ultrason Siemens). Flow velocity was measured in duplicates by doppler (Platon FLO-PRO) and radar (Flodar) sensors.

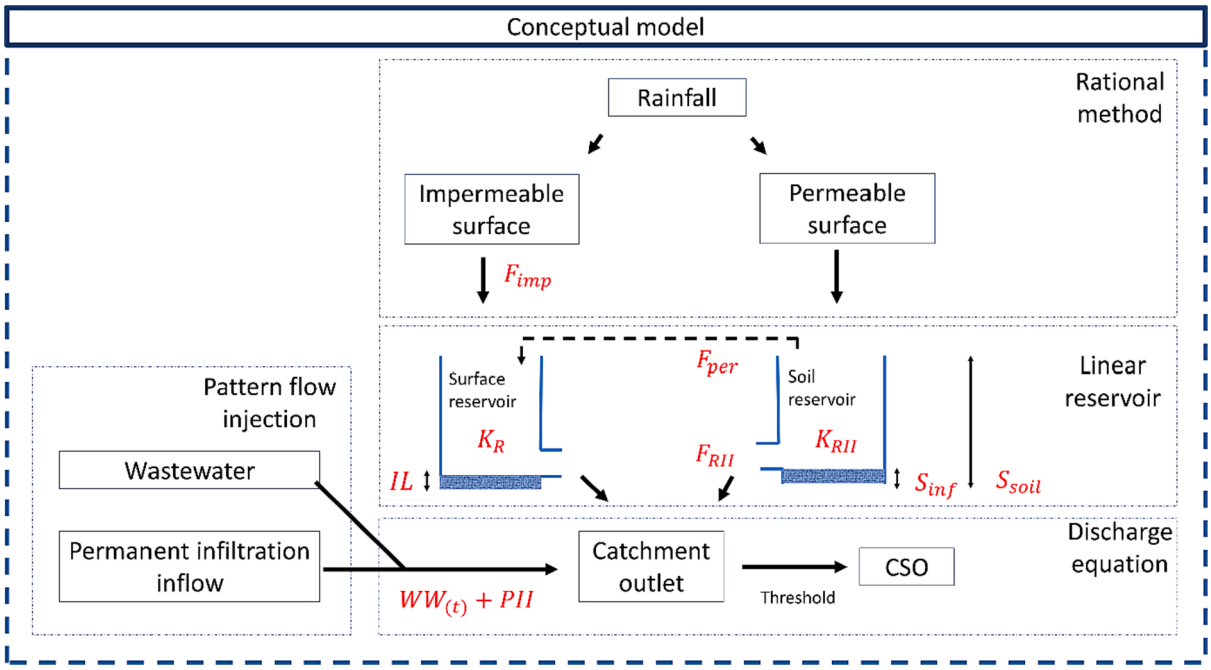

Fig. 3. Schematic diagram of the structure of the conceptual model.

Measurements are taken on the ovoidal pipe located upstream and downstream of the CSOs. Rainfall was measured with a weighing rain sensor (PLUVIO OTT). Measurements were collected at 2-min intervals for water level and flow velocity and 1-min intervals for rainfall intensity.

A rainfall event can be defined as a period of time during which measurable precipitation occurs. The amount of precipitation and the duration of the event can vary. It was defined that a rainfall event is different from another one only if the flow at the outlet returns to the dry weather flow. In our case study, the minimum duration between two consecutive rainfall events is 4 h. From 2007 to 2010, more than 288 rainfall events were monitored, of which 106 induced a CSO event.

2.3. Data pretreatment: Identification of hydrograph components

This section details the different components of the hydrograph observed during the data pretreatment phase. At first, dry weather data was analyzed and the following permanent components were quantified: wastewater varying at the hourly scale with a more or less similar daily pattern during the week, and permanent infiltration inflow (PII), which may vary seasonally. Then, wet weather data was analyzed to observe the rainfall event-based components as: surface runoff, a fast component observed in urban sewer system a few minutes after the beginning of the rainfall event, and rain-induced infiltration (RII), a slow flow component that may be observed up to a few days after a heavy rainfall event.

Dry weather days are defined as days without the influence of surface runoff or RII. In general, there is a fairly regular cycle of daily flows that allows the characterization of wastewater and PII. Complete dry weather daily hydrographs are extracted from long data series (as illustrated in Fig. 2, step 1) to identify the wastewater flow pattern ($WW(t)$) and its characteristics as minimum/maximum flow rates.

Beheshti (2015) and De Bénédittis and Bertrand-Krajewski (2005) have identified several methods to estimate PII based on two principles. The first category of methods estimates the PII baseflow from the difference between the total dry weather flow and the wastewater flow volumes, estimating the latter from drinking water consumption. The second one is based on relating PII to the minimum night-time flow in the daily hydrograph (Kracht and Gujer, 2005). PII is assumed to be constant at the daily scale, and estimated when $WW(t)$ flow should be minimal (and ideally null). PII is therefore taken as the minimum night-time flow in the hydrograph measured at the outlet of the sewer system (generally between 2 and 3 and 4–5 am). Contrary to the first method where two steps are necessary as well as water consumption data, the second method was used in this study as it estimates the PII from one single hypothesis and therefore may result in less uncertainty. Afterwards, PII was considered as a baseflow (Fig. 2, step 2).

The dynamics of the minimum night-time flow was also analyzed over several days after rainfall events. As illustrated by Fig. 2, step 3, it was observed that the minimum night-time flow in sewerage system increases during or immediately after the rainfall event and may take a few days to return to the dry weather flow (PII + $WW(t)$). This "exceedance" flow is attributed to RII water contribution from the soil reservoir which is gradually released into the sewer system.

Subtracting WW(t) and PII from the observed flow at the catchment outlet enables the identification of the wet weather-related flow components (i.e., stormwater runoff and rain-induced infiltration). Their total volume as a function of the total rainfall volume encovers different runoff coefficients depending on the total rainfall. The runoff coefficient being higher when the precipitated volume exceeds a certain threshold, it suggests that impervious surface runoff was not the only surface flow component. Therefore, the pervious surface runoff was also considered. Consequently, as illustrated in Fig. 2, step 4, during a rainfall event, up to three wet weather components were observed in addition to the two permanent dry weather components: surface runoff from impervious and permeable surfaces and RII water.

2.4. Data driven hydrological model description

The elaborated model aims to simulate the key processes of surface runoff and infiltration inflow components at event scale, and evaluate their contribution to combined sewer overflow (CSO) at annual scale. This section presents the key assumptions, hydrological processes, equations and data used.

2.4.1. Conceptual model

The model illustrated in Fig. 3, is a global model with a single spatial entity corresponding to the catchment, conceptually separated into two sub-entities according to the type of surface: impervious and permeable

surfaces, with an area of A_{imp} and A_{per}, respectively. To describe the rainfall-runoff transformation, the rational method was used as production function (Eq. (1)) since it is a simple method with the advantage to have minimal data requirements (Wang and Wang, 2018). The net precipitation flow rate subsequently converted into (1) runoff over impervious surfaces (Q_{imp}), (2) rain-induced infiltration (Q_{RII}, where present), and (3) runoff over permeable surfaces (Q_{per}, where present), is respectively calculated as:

$$Q_{imp}(t) = A_{imp} * C_{imp} * P(t) \quad (1.1)$$

$$Q_{RII}(t) = A_{per} * C_{RII} * P(t) \quad (1.2)$$

$$Q_{per}(t) = A_{per} * C_{per} * P(t) \quad (1.3)$$

where C_{imp} is the runoff coefficient for impervious surfaces, C_{RII} is the rain-induced infiltration coefficient for permeable surfaces C_{per} is the runoff coefficient for permeable surfaces and $P(t)$ is the rainfall intensity at time step t.

At the catchment scale, the equivalent depth of water originating from process i (i.e., the water volume normalized by the total catchment area, A_{tot}), is therefore given by:

$$\frac{1}{A_{tot}} \int Q_i(t)dt = \frac{A_{imp}}{A_{tot}} * C_i * H = F_i * H \quad (2)$$

where H is the total rainfall depth and $F_i = \frac{A_{imp}}{A_{tot}} * C_i$ corresponds to the fraction of runoff that contributes to the flow rate at the global (i.e., catchment) scale, due to (1) runoff on impervious surfaces (F_{imp}), (2) rain-induced infiltration after a rain event (F_{RII}), and (3) runoff on pervious surfaces (F_{per}). For the impervious surfaces, the first millimeters of rain are retained into depression storage which are represented in the surface reservoir as a threshold named IL (for initial losses, Fig. 3). When IL are satisfied, runoff from impervious surfaces begins and thus, the surface reservoir discharge starts.

Permeable surfaces lead to other processes difficult to predict at large scale (Boyd et al., 1993). In the present study, a simplified representation of permeable surfaces was used to conceptualize the hydrological processes before infiltration and runoff. Due to the numerous unavailability of data, evapotranspiration was not modelled in this study.

First, the soil is assimilated to a reservoir with a threshold effect (Fig. 3). When the soil reservoir's capacity exceeds the threshold called S_{inf}, rain-induced infiltration begins, and the fraction F_{RII} is drained by the sewerage system. Once the soil reservoir reaches a second threshold, called S_{soil}, permeable surfaces begin to generate runoff. This process (with a fraction F_{per}) was thus conceptualized as an overflow from the soil reservoir towards the surface reservoir. This study only considers PII and RII contribution from permeable surfaces, even though some authors (Ragab et al., 2003; Ramier et al., 2011) have reported a small fraction of infiltration through impervious surfaces.

The description of the WW(t) flow pattern has been modelled as a constant pattern from one day to another. In the same way, PII is considered as a constant base flow. Dynamic processes are described by two components, both of which are modelled as a linear reservoir: a fast one (surface runoff) characterized by a lag time K_R, and a slow one (rainfall-induced infiltration) with a lag time named K_{RII}. The sum of the previously mentioned components provides the flow rate upstream the CSOs.

Given the variety of CSOs geometries and flow configurations, there are different ways of representing their hydraulic functioning. Several studies, including Andrés-Doménech et al. (2010), Hernes et al., (2020) and Joshi et al. (2021), have determined the CSO rate based on the following condition: if the catchment outflow exceeds the maximum downstream capacity, the CSO rate is equal to excess flow rate. On the other hand, Sitzenfrei et al. (2013) neglected flow dynamics and estimated the CSO volume using a volume balance equation on the

Table 1
Parameter estimation methods.

	Parameter description	Abbreviated name	Method of estimation
Dry weather parameters	Permanent infiltration inflow [L/s]	*PII*	Extraction and statistical analysis of dry weather minimum night-time flow
	Wastewater flow pattern [L/h]	$WW(t)$	Extraction and statistical analysis of dry weather days patterns
Wet weather parameters	Permeable surface storage capacity before runoff [mm]	S_{inf}	Estimated from the correlation between the precipitation depth and the equivalent wet-weather component's depth, is the value separating the impervious surface runoff and beginning of the rain-induced infiltration contribution
	Soil storage capacity [mm]	S_{soil}	Estimated from the correlation between the precipitation depth and the equivalent wet-weather component's depth, is the value that defines the beginning of permeable surface runoff
	Repartition factor of impervious surface [dimensionless]	F_{imp}	Linear regression coefficient of the group considered small rainfalls
	Repartition factor of rainfall-induced infiltration [dimensionless]	F_{RII}	Linear regression coefficient of the group considered medium rainfall minus F_{imp}
	Repartition factor of permeable surface [dimensionless]	F_{per}	Linear regression coefficient of the group considered medium rainfall minus $F_{RII} + F_{per}$
	Initial losses [mm]	IL	Is the maximum rainfall precipitation until there is no runoff volume observed at the outlet
	Lag time of the soil infiltration inflow reservoir [days]	K_{RII}	Fitted parameter from the Eq. (5) and the depletion curve observed for one rainfall event. The mean K_{RII} is retained.
Empirical parameters	Lag time of the surface reservoir [min]	K_R	Empirical value from Desbordes (1974) using the pipe length, and pipe slope, in addition to physical and practical considerations
Catchment and sewer system	Population [habitants]	*Pop*	Municipality data

(*continued on next page*)

Table 1 (*continued*)

	Parameter description	Abbreviated name	Method of estimation
characteristics parameters	WW production per capita [L/hab/day]	*EH*	Municipality data
	Catchment area [ha]	A_C	Geographic information system: aerial images treatment
	Impervious area [ha]	A_{IMP}	Geographic information system: aerial images treatment
	Main drain slope [%]	*I*	Sewer system plans
	Length of the longest water route [m]	*L*	Sewer system plans

maximum wastewater treatment plant volume capacity and the sewer volume produced in the catchment. In this case study, the CSOs is not frontal or lateral which represents a modelling challenge. None of the previously mentioned approaches could be employed. A prior study by (Momplot, 2014) utilized a 3D model to analyze the hydraulic behavior of the CSOs. Through numerical simulations, the CSO threshold was identified (Eq. (3)). Additionally, the CSO rate was ascertained as a non-linear function of the upstream flow rate (Eq. (4)). The CSO volume was then estimated by integrating Eq. (4) over the time.

$$Q_{CSO}(t) = 0, \text{when } Q(t) < 0.4\, m^3.s^{-1} \quad (3)$$

$$Q_{CSO}(t) = Q(t) - 0.33*\ln(Q(t)\ ) - 0.69\,, \text{when } Q(t) > 0.4\, m^3.s^{-1} \quad (4)$$

where $Q(t)$ $[m^3.s^{-1}]$ is the flow rate upstream the CSO and $Q_{CSO}(t)\left[m^3.s^{-1}\right]$ is the CSO rate at the time step t.

2.4.2. Parameter calibration

The model requires ten input data to be estimated (described above and shown in red in Fig. 3). For nine of them, this is achieved through the analysis of observed data and the last one (K_R) is estimated via an empirical equation. In addition, six other parameters describe the characteristics of the catchment. The detailed list of all parameters used in the model is presented in Table 1. The following section describes in detail the methods used for each parameter calibration with observed data.

Three years of observation (2007 and 2009–2010) were taken in order to have enough data to calibrate the parameters. For the model evaluation, an intermediate year (2008) was reserved to avoid any influence on the simulations due to changes in the territory.

The daily wastewater flow patterns ($WW(t)$) were derived from the observed data collected during the selected period of 2007, 2009 and 2010. All the patterns obtained during the study period were examined and the median hourly flow rate was retained to reconstruct a median daily wastewater flow pattern ($WW(t)$) with hourly time step. In the same way, permanent inflow infiltration (PII) has been identified through the observations of the minimum night time flow during all dry periods. An inter-seasonal minimum night-time flow comparison, corresponding to the four typical European weather seasons, was carried out to observe a potential seasonal variation of PII, i.e., due to differences in the groundwater level or in the soil moisture, but there was no significant difference between the estimated PII between seasons (Appendix 1), thus, the base flow was considered to be the same throughout the year.

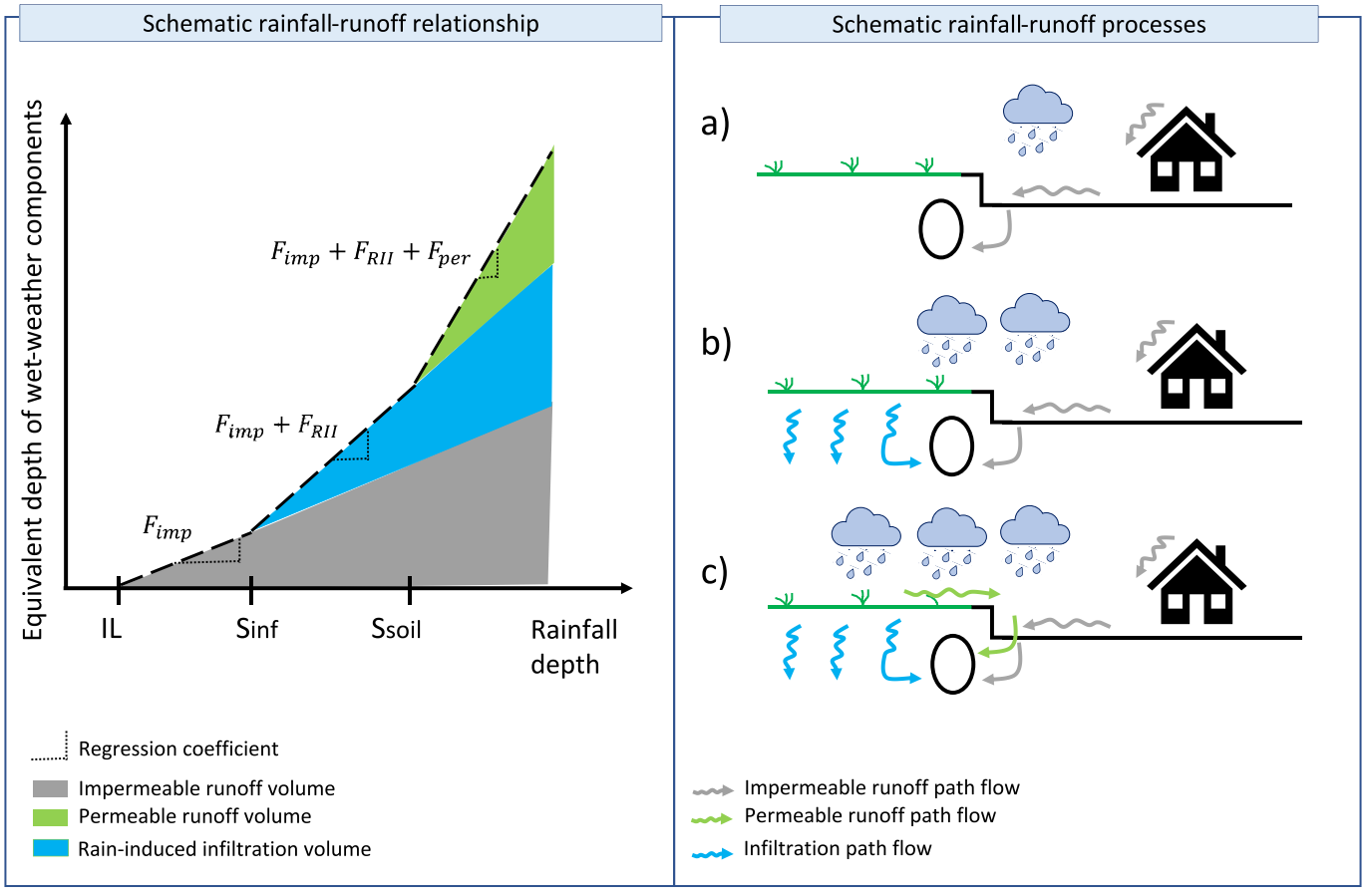

Fig. 4. Schematic rainfall-runoff relationship (left) and conceptualization of the rainfall-runoff processes (right).

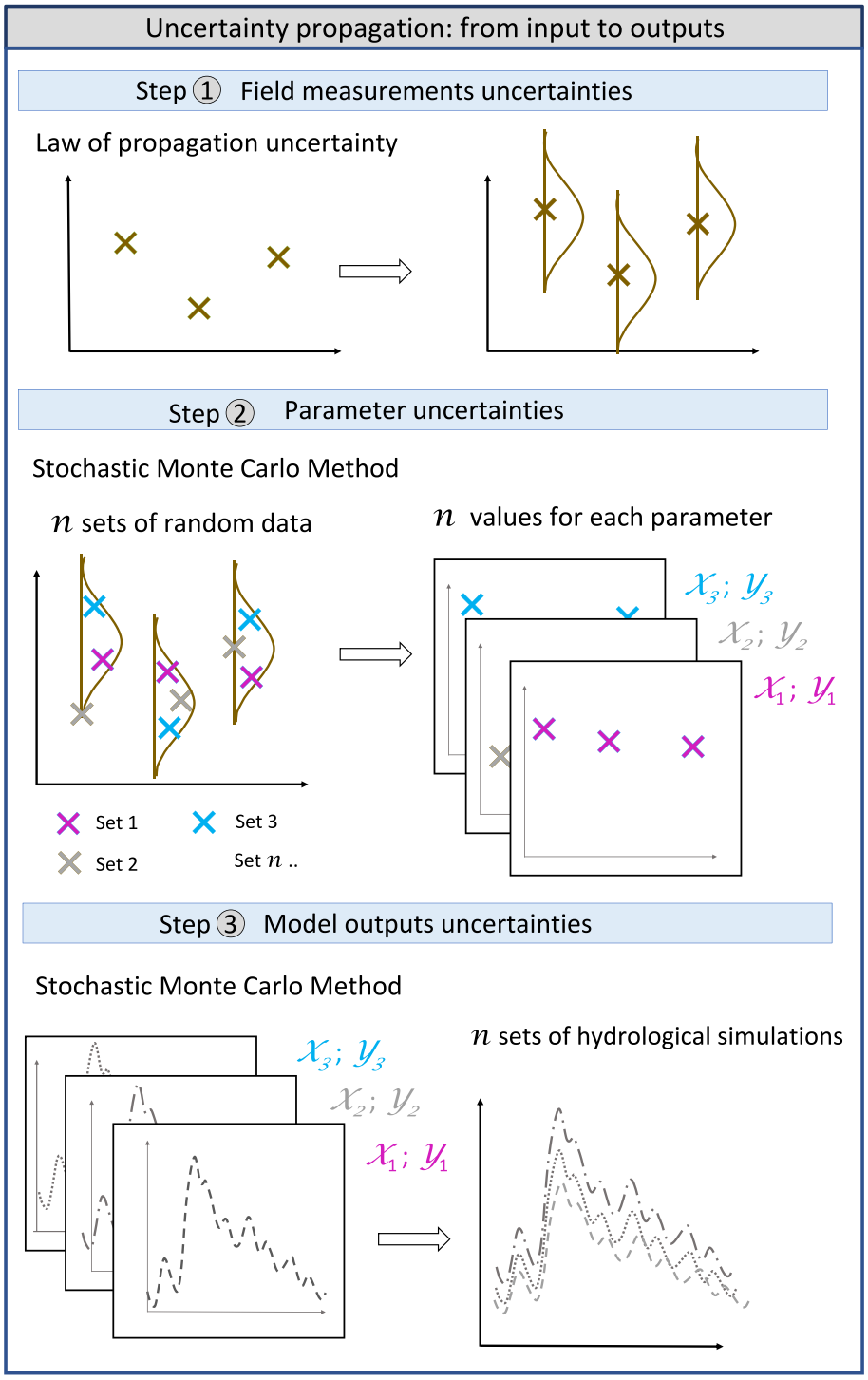

Fig. 5. Methodology used for propagating uncertainties from input data to model outputs.

For all the events in the 2007, 2009 and 2010, the equivalent depth of wet-weather flow was calculated and plotted against the rainfall depth as shown in Fig. 4. The resulting scatterplot shows three distinct groups of points, each having its own slope. This differentiation supports the assumption that depending on the rainfall depth, different hydrological processes are present based on the rainfall depth (i.e., runoff on impervious surfaces, rain-induced infiltration after a rain event, and runoff on permeable surfaces). According to Eq. (2) there is a linear relationship between the total volume observed at the catchment's outlet and the rainfall depth. This can be observed in Fig. 4 by three different slopes, respectively, F_{imp}, $F_{imp} + F_{RII}$ and $F_{imp} + F_{RII} + F_{per}$.

Three linear regressions were implemented, whose slopes directly provide the values of fractions F_{imp}, F_{RII}, F_{per}. The intersection of the first line with the x-axis corresponds to the initial losses (IL). The *abscissas* of the slope changes define the thresholds S_{inf} and S_{soil} (Fig. 4).

The rainfall-runoff relationship provides information on the fraction of impervious surface runoff, rain-induced infiltration and permeable surface runoff. The physical processes associated with each fraction and their order of arrival in the sewer system is illustrated in the schematic rainfall-runoff processes for a a) small, b) medium and c) heavy rainfall event (Fig. 4).

In order to estimate the lag time K_{RII}, the observed depletion curves

of the infiltration inflow, discharged from the soil after heavy rainfall events, were used to describe the gradual release of the soil reservoir. If the infiltration from the soil to the sewer system is represented by a linear reservoir model, with a lag time K_{RII}, then the depletion curve after a rain event should follow an exponential decrease towards the baseflow (Eq. (5)).

$$Q_{night}(t) = \left(Q_{night}(0) - PII\right)*e^{-\frac{t}{K_{RII}}} + PII \quad (5)$$

where t is the t^{th} day after the rainfall event, $Q_{night}(t)$ is the average flow between 3 and 4 am observed on day t, $Q_{night}(0)$ is the value observed between 3 and 4 am immediately after the rainfall event, PII is the permanent infiltration inflow, and K_{RII} the lag time of the soil reservoir.

The value of the three parameters, $Q_{night}(0)$, PII, and K_{RII}, was optimized for each heavy rainfall for which the decrease of $Q_{night}(t)$ (the observed depletion curve) was visible during several days after the beginning of the rainfall event. Optimization was carried out through non-linear regression with a classical least squares objective, applying Eq. (5) to the observed data. The inter-event variability of the parameter of interest, K_{RII}, was subsequently analyzed via descriptive statistics.

To describe the response of impervious and permeable surfaces to rainfall events, the surface runoff lag time (K_R) was calculated from the catchment characteristics using the empirical formula of Desbordes (1974) (Eq. (5)). There appears to be some variability between the estimations made with other empirical equations (Appendix 2). Therefore, the values provided by each of these equations were compared and the min–max range value were extracted to define the range of K_R interval.

$$K_R = 5.3*{A_C}^{0.3}*\left(\frac{A_{imp}}{A_C}\right)^{-0.45}*I^{-0.38}*L^{0.61} \quad (6)$$

where A_C is the catchment area (ha), $\frac{A_{imp}}{A_C}$ is the impervious fraction of the catchment, I is the average slope (%) and L the length of the longest water route (main drain, m). The exponents were determined through optimization method in Desbordes (1974) fitting experimental data from 146 rainfall events in 13 French and American catchments.

2.5. Uncertainties propagation: From observed data to model simulation

Being a data-driven approach, this model and most of its parameters are based on observations (rainfall and flow rate) which are themselves determined with some uncertainties.

Several parameters used in the simulation were derived from depth, velocity, and rainfall measurements with uncertainties. These uncertainties come from many factors, such as measurement errors (precision and accuracy inherent to the sensors itself), environmental uncertainty (this refers to uncertainty due to temperature or pressure changes that can affect sensors reading), human error and random noise (random fluctuations in the sensor data). They were accounted for the law of propagation of uncertainty (Bertrand-Krajewski et al., 2021). Each measured flow rate was described as a random variable following a normal distribution centered on the measured value (Fig. 5, step 1).

Then, the stochastic Monte Carlo Method (MCM) was used to propagate these uncertainties to each model parameter determined from flow rate measurement. The previous estimation procedure was applied to 10^4 sets of random data sampled from the respective distribution leading to 10^4 possible values for each parameter (Fig. 5, step 2). Applying a similar method, 10^4 hydrological simulations were performed to calculate the resulting uncertainty on the model outputs (Fig. 5, step 3).

2.6. Model accuracy evaluation

A series of twenty events that occurred in 2008 with CSO events were randomly selected (listed in Appendix 3). The model's accuracy was evaluated in three steps. First, the Kling-Gupta Efficiency (KGE, Eq. (7)) was used as a goodness of fit criteria (Gupta et al., 2009) to assess the model's ability to simulate the observed flow rate at the sewer system outlet.

$$KGE = 1 - \sqrt{(r-1)^2 + (\alpha-1)^2 + (\beta-1)^2} \quad (7)$$

where r is the Pearson product-moment correlation coefficient between simulations and observations, $\alpha = \frac{\sigma_s}{\sigma_o}$ is a measure of the flow variability error between the observed (σ_o) and simulated (σ_s) standard deviations, and $\beta = \frac{\mu_s}{\mu_o}$ is a measure of the flow error between the observed (μ_o) and simulated (μ_s) flow means over the selected events. The KGE ranges from 1, as a perfect simulation, to minus infinity. Kouchi et al., (2017) proposed that the KGE can be considered indicative of a well-performing model if it is equal or greater than 0.75. For a model to be considered with an acceptable level of performance, the KGE values must be at least 0.5.

Second, the difference between observed and simulated CSO volume was considered to evaluate the model's performance for the selected twenty rainfall events. Third, the model's ability to replicate the CSO frequency was assessed.

2.7. Scenario elaboration

The contribution of Permanent Infiltration Inflow (PII) and Rain-Induced Infiltration (RII) on CSO has been assessed by modelling two scenarios: i) a reduction of 50 % of PII and RII; ii) a completely of PII and RII. Achieving these outcomes through a strategic approach necessitates a comprehensive understanding of the origin of the infiltration inflow and the study site (i.e., targeted pipeline renewal). Scenario analysis was studied at a yearly scale over four years (2007, 2008, 2009 and 2010) and on an event-based scale through 3 heavy rainfall events with a 1-min resolution. To determine the contribution of PII and RII on CSO in the long and short term, two points of the sewer system were analyzed: the upstream and downstream pipe of the CSOs. For both temporal scales, a first distinction was made between the different components in the outflow to quantify the impact of PII and RII. Then, the contribution of PII and RII to CSO was assessed through the total CSO volume, CSO duration, CSO frequency and CSO rate. The three indicators' results were compared to the results obtained through the simulation of the *status quo*. The difference is attribute to the contribution of infiltration inflow component. The results are presented as rates of change for both scenarios.

A recurring question in urban water management is whether to continue with centralized systems by rehabilitating sewer systems, and thus reduce infiltration-inflow, or to pursue decentralization (Arora et al., 2015; Libralato et al., 2012). To compare the effectiveness of stormwater disconnection in reducing CSO volumes, two complementary scenarios were developed in addition to the previous ones. These scenarios aim to disconnect stormwater from the combined sewer system by implementing source control structures for stormwater management such as green roofs, rain gardens and swales that collect water from nearby roofs and pavements. These structures capture and infiltrate rainwater, reducing a fraction of surface runoff. To model stormwater disconnection scenarios, the initial loss values of the surfaces on which these structures could be implemented were increased to conceptualize the capacity of the structures to store and infiltrate the first millimeters of rainfall. There is a possibility that water infiltrating through the SUDS could reach the sewer system. However, in the absence of experimental data to parameterize this phenomenon, it will not be considered. Two scenarios were conducted, increasing initial losses by 5 and 10 mm. The CSO volume reduction was used to compare the infiltration inflow reduction and the disconnection scenarios through four years of simulations.

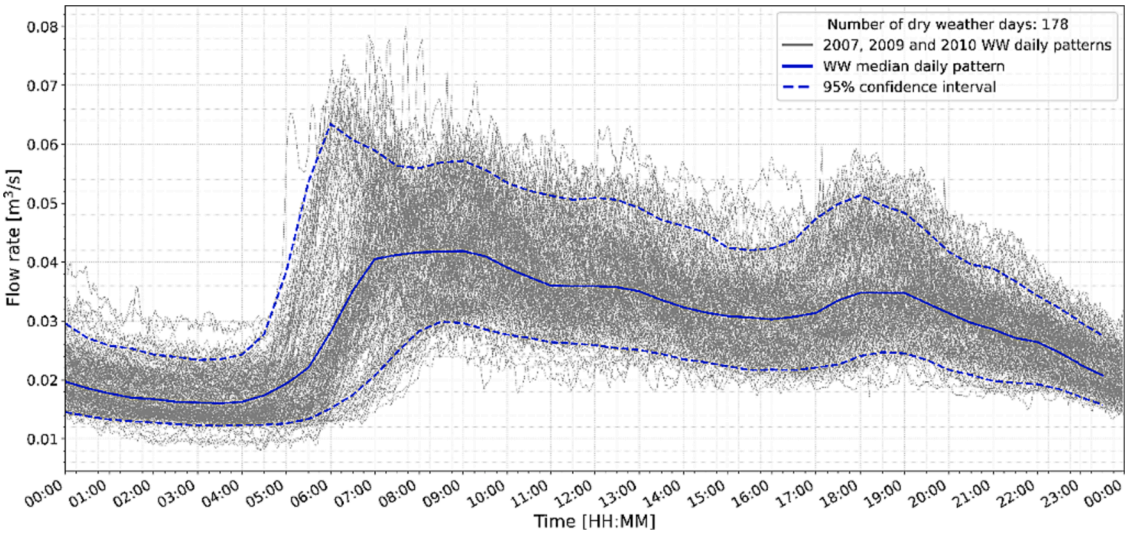

Fig. 6. Daily variation of wastewater pattern 2007, 2009 and 2010 in Ecully Catchment.

Table 2
Estimated value and range for each model parameter.

Parameter description	Abbreviated name	Estimated value	Lower bound (5 %)	Upper bound (95 %)	Type of distribution	Number of events used for parameter estimation
Permanent Infiltration Inflow [L/s]	PII	19	14	24	Uniform	178 dry weather days
Initial losses [mm]	IL	1.75	0.5	3	Uniform	95 rainfall events and literature data
Vegetation coverage and soil storage capacity [mm]	S_{inf}	15	13	17	Uniform	95 rainfall events
Maximum soil storage capacity [mm]	S_{soil}	35	30	40	Uniform	95 rainfall events
Repartition factor of impervious surface [dimensionless]	F_{imp}	0.135	0.13	0.14	Normal	76 rainfall events
Repartition factor of rainfall induced-infiltration [dimensionless]	F_{RII}	0.095	0.05	0.14	Normal	11 rainfall events
Repartition factor of permeable surface [dimensionless]	F_{per}	0.115	0.09	0.14	Normal	8 rainfall events
Lag time of the soil infiltration inflow reservoir [days]	K_{RII}	1.2	0.5	1.9	Uniform	13 depletion curves coming from 13 different rainfall events
Lag time of the surface reservoir [min]	K_R	10	10	37	Uniform	Empirical formula from Desbordes (1974).

3. Results

3.1. Identification of parameters ranges

Dry weather days from 2007, 2009 and 2010, were extracted to identify the median annual wastewater flow pattern. Fig. 6 shows the superposition of 178 complete flow patterns measured in dry weather, with maximum peaks in the morning and evening and a minimum peak late-night. Minimum flow occurs during the night, around 3 and 4 am, which is identified as PII as presented in the Materials and Methods section. Statistics about PII values are extracted from all monitored dry days: the median PII of 19 L/s was retained with a variability between [14 L/s; 24 L/s] as shown in Table 2.

The linear correlation between precipitation volume and runoff volume was calculated for 95 rainfall events observed in 2007, 2009 and 2010 (Fig. 6). Three groups with, respectively, 76, 11 and 8 rainfall events were observed and categorized in accordance with the theoretical part (section 2.4.2 Parameter calibration). The respective repartition fractions of F_{imp}, $F_{imp} + F_{RII}$, and $F_{imp} + F_{RII} + F_{per}$ were associated to the regression coefficient of each group (Fig. 7). Thus, median values of 0.135, 0.095 and 0.115 with an interval of confidence (Table 2) were assigned to the respective fractions of F_{imp}, F_{RII} and F_{per}. The boundary between the three groups was estimated graphically from Fig. 6, which showed ranges of 13 – 17 mm and 30 – 40 mm. Respectively, the parameters S_{inf} and S_{soil} were associated to these ranges.

Initial losses for impervious surfaces were estimated taking into consideration the catchment slope and surface (Boyd et al., 1993; Kidd, 1978; Rammal and Berthier, 2020). Typical values of initial losses in similar urban catchments were already observed (Leopold, 1991; Rao and Delleur, 1974) leading to an extended range between 0.5 and 3 mm (Table 2). Likewise, the surface lag time (K_R) was estimated to be 10 min using the empirical formula of Desbordes (1974). This value was compared with those calculated using the other empirical equations (i.e., Chocat, (2013) and Desbordes and Ramperez (1977) provided in Appendix 2). From this comparison, the min–max range of values (10 and 37 min respectively) were used to construct the uniform distribution (Table 2).

To determine K_{RII}, the depletion curves of rainfall events bigger than S_{inf} were analyzed, between them, 11 events were retained over the years 2007, 2009 and 2010. Equation (5) was fitted to the data corresponding to the observed minimum flows between 3 and 4 am using a nonlinear regression approach as shown in Fig. 8. For the depletion curves retained, values ranging from 0.45 and 2.6 days were obtained. The median K_{RII} was retained with a confidence interval of [0.5–1.9] days as shown in Table 2.

3.2. Model accuracy evaluation

A set of twenty rainfall events from 2008 (Appendix 3) was used to evaluate the model by incorporating parameter values calibrated using

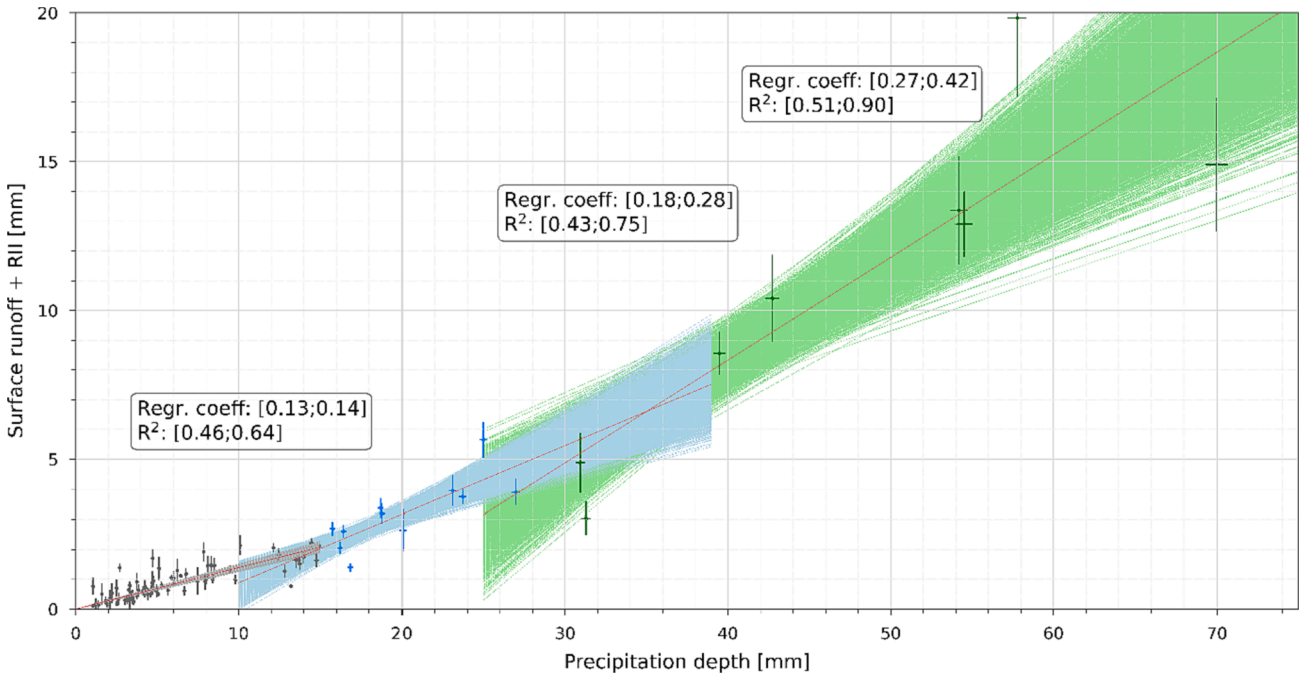

Fig. 7. Relationship between the precipitation depth and the runoff depth (surface runoff and rain-induced infiltration) for three rainfall groups. The linear regressions are derived from observed points uncertainties. Three clusters are identified by different colours: the first one in grey colour is attributed to the impervious surface contribution, the second one in light blue colour is attributed to the addition of impervious surface runoff and rain-induced infiltration, and the last one, in light green to the addition of impervious surface runoff, rainfall-induced infiltration and permeable surface runoff. (For interpretation of the references to colour in this figure legend, the reader is referred to the web version of this article.)

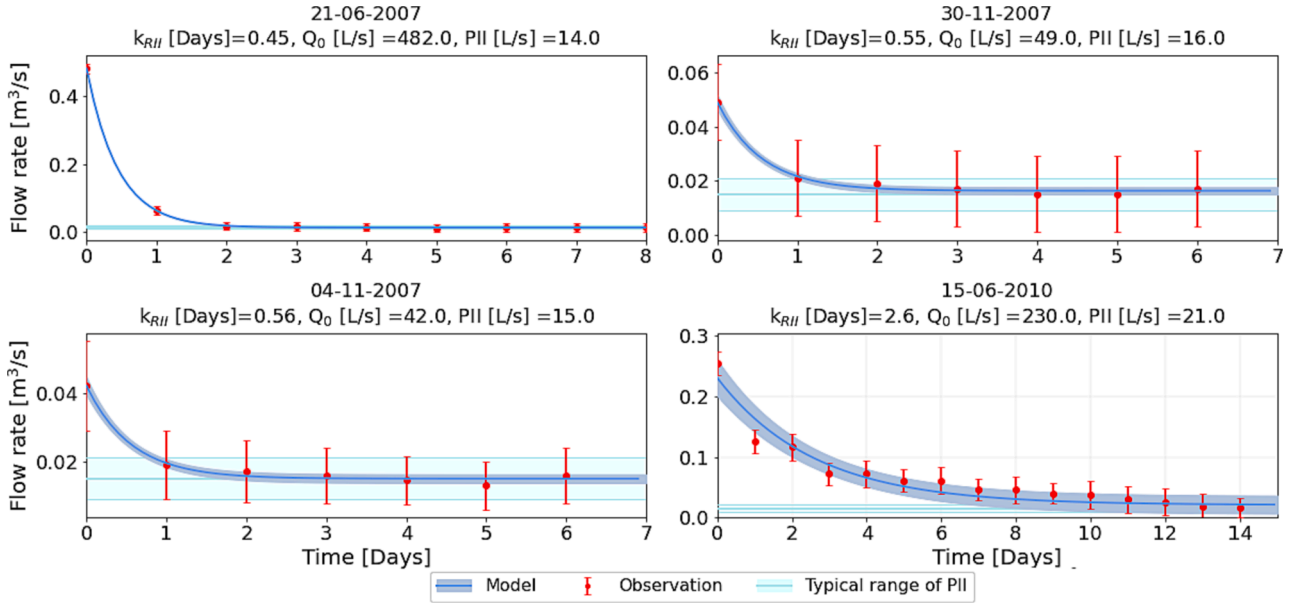

Fig. 8. Rainfall-induced infiltration lag time (K_{RII}) optimization. The x-axis represents the number of days after the end of the rainfall event, starting at $Q_{night}(0)$ (Eq. (5)), which is the value observed immediately after the rainfall event. The y-axis corresponds to the observed flow rates which correspond to the minimum flow rate between 3 and 4 am after the rainfall event. The red dots represent the observed flow rate with its uncertainties, the horizontal light-blue line is the typical range of Permanent Infiltration Inflow (PII) with its 90 % confidence interval and the blue line is the depletion curve with its confidence interval. (For interpretation of the references to colour in this figure legend, the reader is referred to the web version of this article.)

data from 2007, 2009 and 2010. The model's evaluation resulted in KGE values greater than 0.6 for 90 % of the ensemble of parameter sets (Appendix 4), the other 10 % range from 0.45 to 0.60. To illustrate the hydrographs simulated upstream the CSOs, Fig. 9, presents six examples of rainfall events where events 5 and 6 are small rainfall events, events 11 and 13 are medium rainfall events and events 18 and 19 are big rainfall events. The twenty rainfall events simulated are present in Appendix 5, 6, 7. The model shows the capability to provide a satisfactory flow variation with a good simulation of the peak values and the depletion curve for almost all events. It may happen that some events are not well reproduced by the model. First, some modelled peak values were underestimated when the precipitated depth increases very quickly

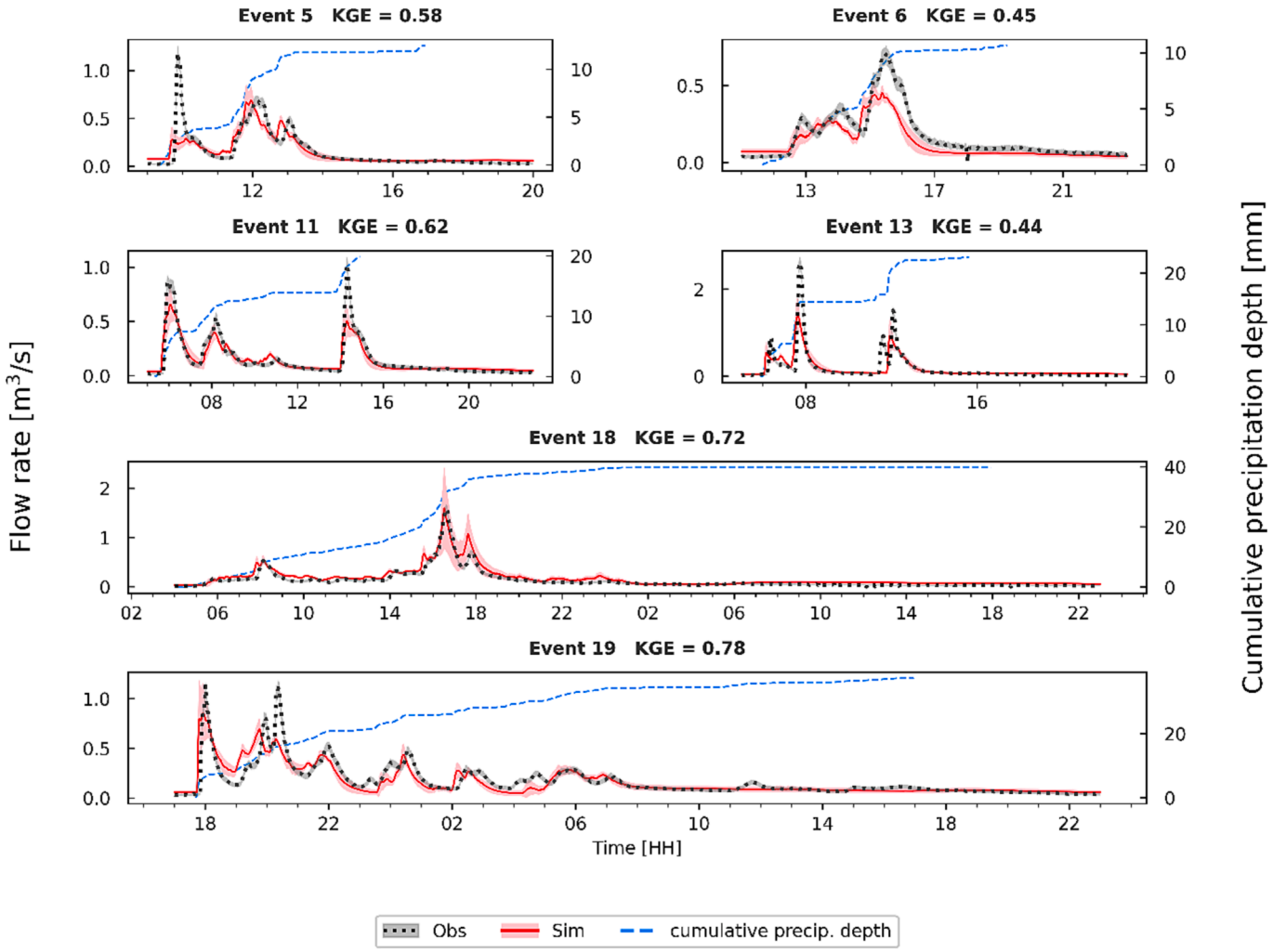

Fig. 9. Validation results for 6 rainfall events. The red line and pink coverage represent the medium-simulated hydrograph and the uncertainties related to the 10^4 sets of input parameters. The black-dotted hydrograph represents the observed flow rate at the outlet of the catchment. The dashed blue line represents the cumulative precipitation depth corresponding to the right axes. (For interpretation of the references to colour in this figure legend, the reader is referred to the web version of this article.)

as shown by event n° 5 at 10 am and event n° 11 at 3 pm. Second, some events as event n° 3 and event n°4 in Appendix 5 are not well reproduced. This could be due to local rainfalls that are not register in the rain gauge or hydraulic processes that are not represented as the back water curve variation in the main sewer pipe. However, even if some events are not well reproduced, the set of events gives satisfactory KGE value and for almost all the events the upstream CSO hydrograph gives a satisfactory shape for the objectives of the model.

The simulated and observed CSO volumes were compared in Fig. 10. The most frequent situation corresponds to an underestimation of the CSO volume by a few tens to a few hundred m^3. For several rainfall events, however, the model was found to either underestimate or overestimate the CSO volume by 10^3 m^3 or more (Fig. 10).

Overall, if these values are considered from an annual perspective, the total simulated CSO volume matches the observed value relatively well (Fig. 10), but this is partly the result of compensation between cases of under- and over-estimation. By consequence, the relative error for the CSO volume is minimal, at 4.9 % (Table 3). In addition, out of the 20 CSO events observed, 19 were simulated (Event4, Appendix 5, was not simulated even considering uncertainties).

This reflects the good capacity of the model to reproduce the total CSO volume and CSO frequency over the ensemble of events and therefore concludes that the model is suitable to evaluate possible planning scenarios in an annual perspective. Assessing the contribution of PII and RII to CSO volume.

The results of the annual simulation aim to evaluate the influence of Permanent Infiltration Inflow (PII) and Rain-induced Infiltration (RII) flow components on CSO in the study area. The contribution of urban components in the annual outflow volume of the sewer system (volume upstream the CSOs) was compared in the PII and RII reduction scenarios (i.e., reduction of 0, 50 and 100 % of PII and RII). The annual water balance for all years studied (from 2007 to 2010) shows that the component contributing the most to the annual scale volume produced is wastewater, followed by PII and RII and surface runoff with a mean contribution of ~53, ~37 and ~10 %, respectively (Appendix 8). Regarding the effect of a partial reduction of PII and RII, a decrease of ~24 % of PII and RII could be achieved (Appendix 8).

The CSO duration and CSO rate of all CSO events that occurred from 2007 to 2010 were also compared. Whatever the PII and RII reduction scenarios considered, no significant differences were found in the changes in the CSO duration or the CSO rate. This can be attributed to the fact that 60 % of CSO event were triggered by small rainfall events (rainfall depth < 15 mm), which is not expected to generate RII. Indeed, the CSO rate is attributed to fast surface flows such as runoff from permeable and impervious surfaces.

The reduction of the annual CSO volume for the four years (from

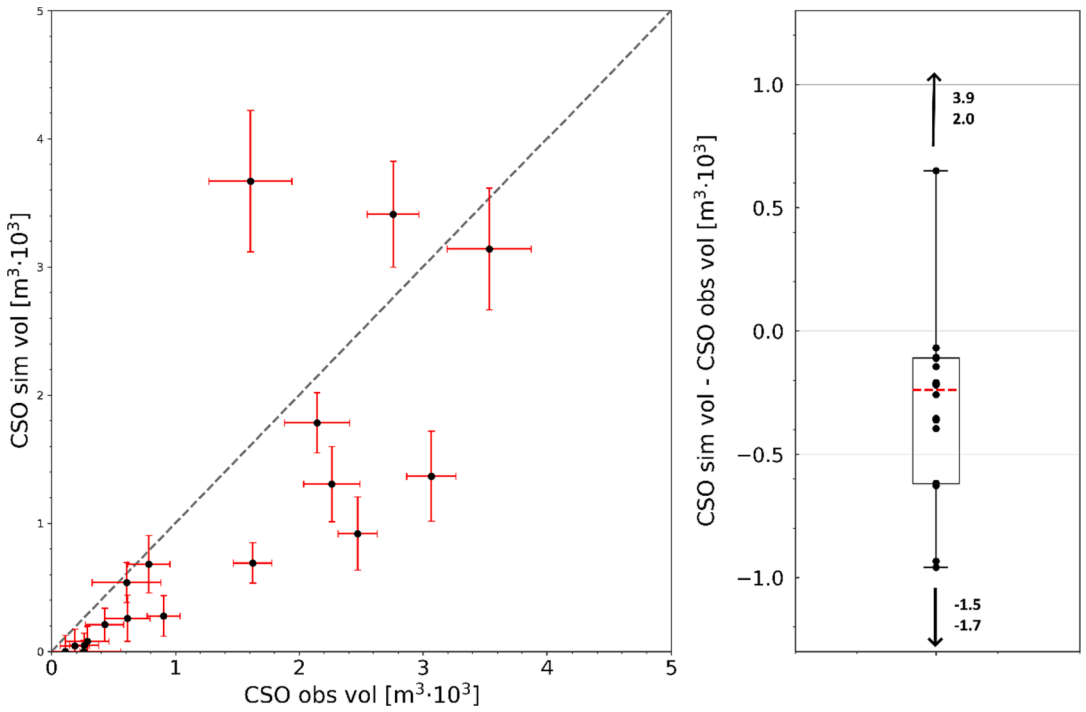

Fig. 10. Comparison between simulated and observed CSO volumes for 20 rainfall events in 2008.

Table 3
Comparison of CSO volumes over the 20 rainfall events selected in 2008.

Observed CSO volume (m^3)	44 400 ± 3 900
Simulated CSO volume (m^3)	42 200 ± 6 100
Error (%)	5 %

2007 to 2010) was studied and shows that PII and RII have a clear effect on the CSO volume. For a PII and RII reduction of 50 %, simulations show that the annual CSO volume may decrease between 5 and 7.5 % (Appendix 9). On the other hand, the total reduction of PII and RII shows that the maximum possible contribution of this component in the CSO volume could represent from 11 to 16 % (Appendix 9). However, despite the partial or total removal of these two components, the CSO frequency is the same in both scenarios and the baseline one for all years except 2009. In that year, due to the rainfall characteristics (long event with a low peak flow), the CSO frequency decreased by one and two days, respectively, for a reduction of 50 and 100 % of PII and RII.

The effect of PII and RII reduction for 3 heavy rainfall events has been simulated and illustrated in Fig. 11. At the event scale, PII and RII could represent almost 24 % of the volume at the outlet of the system. Considering a 100 % PII and RII reduction, 18 to 24 % of the volume at the outlet is reduced and the CSO volumes was reduced from 13 to 18 % (Fig. 11). A qualitative hydrograph analysis shows that PII and RII reduction slightly decreases the peak flow which confirms that this indicator does not seem relevant for this component.

3.3. Comparison of PII and RII reduction and disconnection scenarios impact on CSO volumes

Fig. 12 illustrates the reduction in CSO volume for the four scenarios (i.e., the PII and RII reduction of 50 and 100 % and disconnecting the first 5 and 10 mm of the rainfall event) over all the rainfall events that occurred between 2007 and 2010. Results indicate that disconnecting the first 5 mm of rain could lead to a reduction from 13 to 48 % of CSO volume for half of the CSO events. Furthermore, disconnecting the first 10 mm of rainfall could lead to suppressing half of the CSO events.

Concerning the reduction of PII and RII scenarios (Fig. 12), a partial reduction of PII and RII would lead to a reduction of CSO volume over 4 years by 5 to 10 % for half of the CSO events. For a total reduction scenario, the CSO volume would be reduced by 10 to 18 % for half of the events. These results seem to be consistent with the annual results of Appendix 9.

4. Discussion

4.1. Consistency between calibrated parameters and physical values

The model is characterized by its integration of monitoring data and empirical equations, reflecting a parsimonious approach despite the complexity of the urban catchment and its sewer system. It provides an accurate simulation of the quantity and dynamics of different water components within the catchment. The method used to calibrate the model from observed data at the catchment outlet has resulted in reliable parameter estimates, providing reasonable physical intervals for all parameters.

In this case study, the available data used to calibrate the heavy rainfall event parameters and their uncertainties were relatively limited. Despite this, the values found for the threshold before the beginning of the rain induced infiltration, S_{inf}, are similar to values found in experimental studies of urban vegetation surfaces such as Asadian and Weiler (2009) who estimated an interception of 70 % for rainfalls of ~25 mm and ~15 h, or Armson et al. (2013) in the United Kingdom who showed that for rainfalls of 10 mm, a single tree can reduce pavement runoff by 25 % and a lawn can completely eliminate surface runoff.

For the single empirical parameter (surface lag time, K_R) we decided to explore the validity of the estimated values. For this purpose, the empirical formulas modified by Chocat (2013), Desbordes (1974), Desbordes and Ramperez (1977) were compared with a sensitivity analysis of K_R. Firstly, the values obtained with the selected empirical formulas ranged from 10 to 37 min (Appendix 2). Secondly, for the K_R sensitivity analysis, the optimum parameter set from the MCM simulations during the model accuracy evaluation (section 1.2 Model accuracy

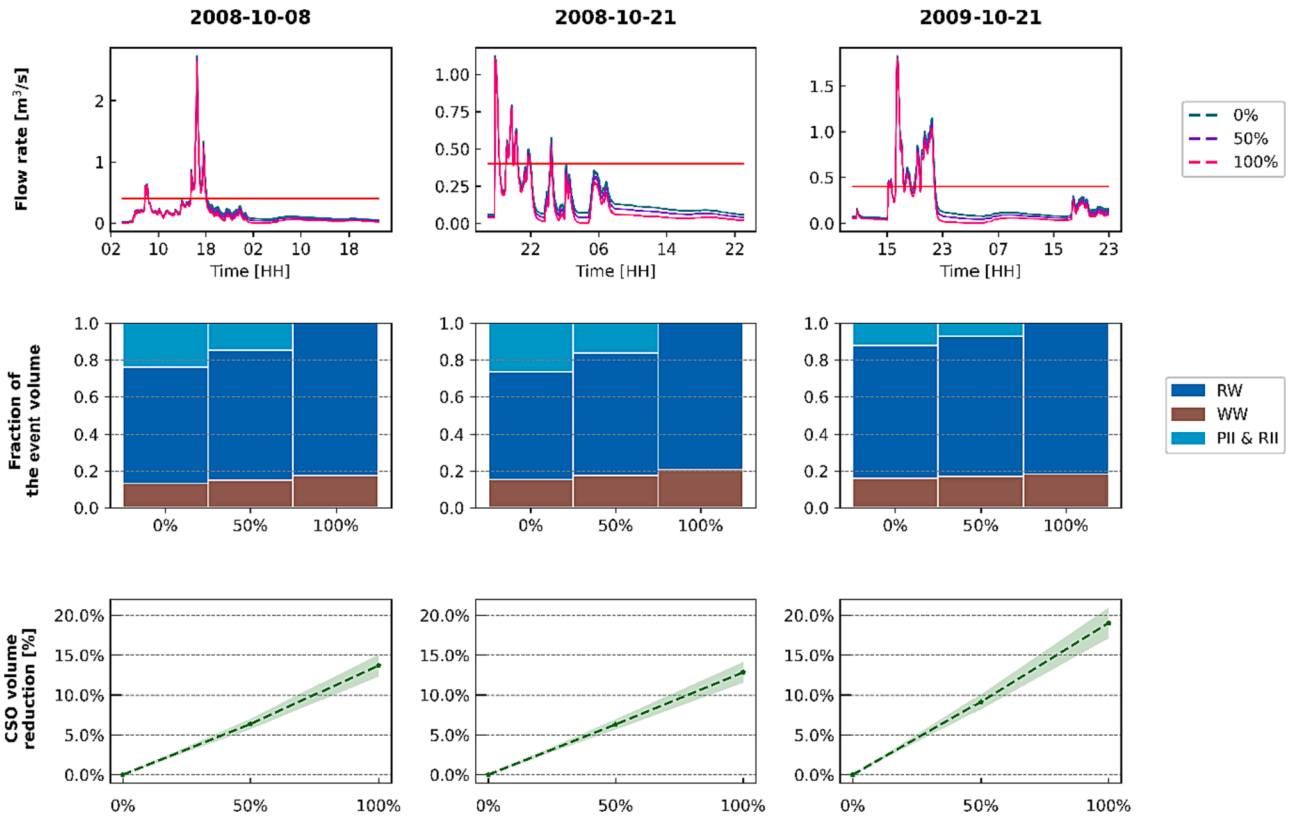

Fig. 11. Impact of permanent infiltration inflow and rain-induced infiltration (PII and RII) reduction for three heavy rainfall events. In the 1st row the impact on the flow rate dynamic. The 2nd row shows the water balance at the sewer system outlet. The 3rd row presents the CSO volume reduction.

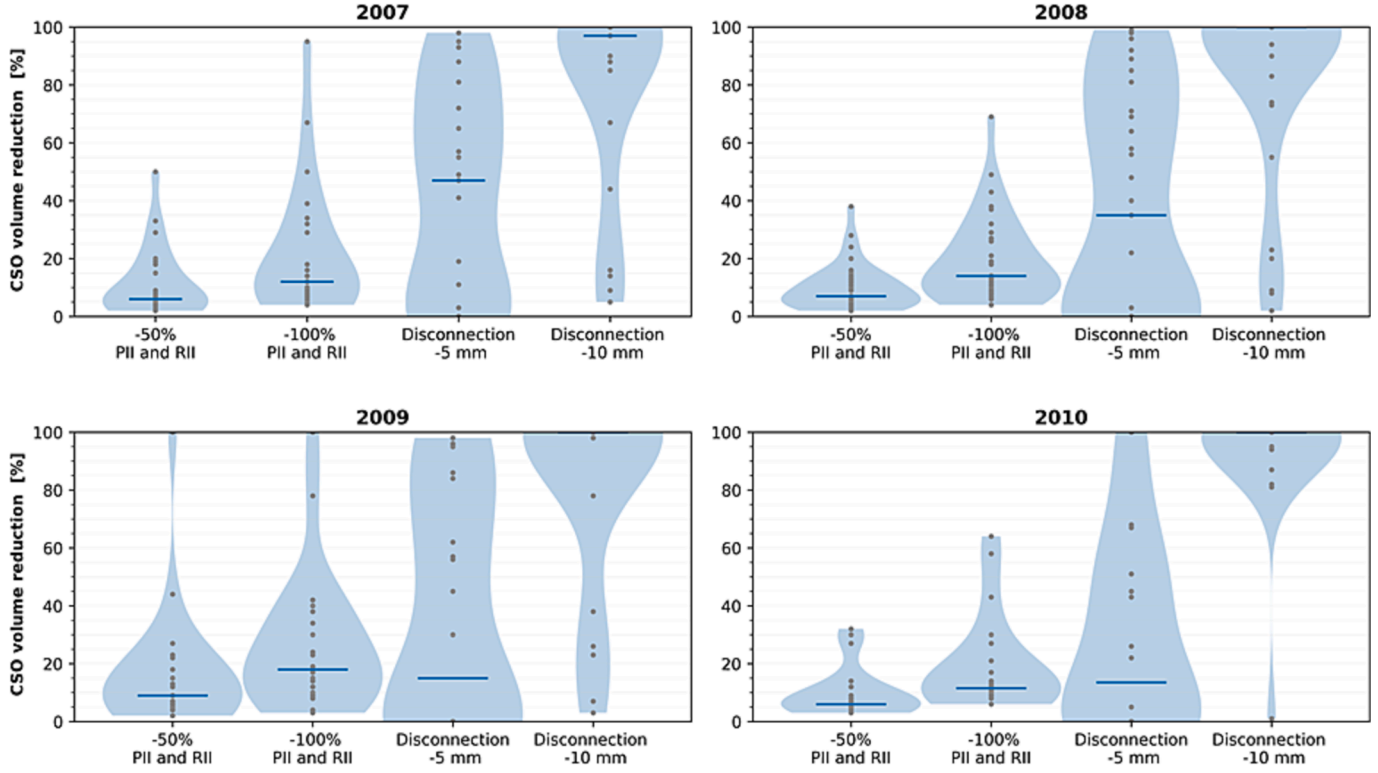

Fig. 12. CSO volume reduction for four different scenarios. Two permanent infiltration inflow and rain-induced infiltration (PII and RII) reduction scenarios were considered, a partial and complete reduction of PII and RII of the sewer. Two disconnecting scenarios: infiltrating the first 5 and 10 mm of surface rainfall runoff. Four years were simulated (from 2007 to 2010). The CSO volume reduction is represented by violin plots displaying the distribution and density of the data at different values. The data represent all rainfall events that occurred during the study years which resulted in a CSO event.

evaluation) was retained and only the K_R parameter was modified with values ranging from 5 to 100 min. A sensitivity analysis was carried out to assess the reliability of these extended ranges of values on the indicator used for model evaluation (KGE coefficient applied to 25 rainfall events). Variations in KGE resulting from the changes in K_R when applying different empirical formula were found to be smaller than the variations due to the other uncertain parameters and especially the runoff coefficients (Appendix 10).

4.2. Feasibility and consequences of evaluated scenarios

Regarding the modelling scenarios, as permanent infiltration inflow information is rarely available with a high spatial resolution, modelling a targeted reduction of PII and RII is not possible. In those cases, the model has been shown to be promising as it helps to quantify the initial situation and to simulate scenarios, before investing large efforts in targeted studies.

In the present study, PII and RII components were estimated as the second major component of the sewer system at the annual scale (~38 % of the total volume). In addition, the results of the PII and RII scenarios implemented in this study suggest that PII and RII could contribute from 13 to 24 % of the annual CSO volume, which could reduce additional costs due to water infiltration into the sewer system (Dirckx et al., 2019). In previous studies, RII and PII accounted for 24–47 % of the total water volume in combined sewer (Bentes et al., 2022; Pangle et al., 2022; Weiß et al., 2002) and up to 35 % of the CSO volume (Dirckx et al., 2019). The proportion of the flow volume seems to be similar to the observation in existing literature despite the highly variable characteristics of each case study.

Removing PII and RII may reduce the CSO volume but does not seem to have a significant impact on CSO frequency, which is consistent with findings from Schulz et al. (2005). This limitation may be problematic for the receiving environment because reducing volume alone may not guarantee improvements in river quality, and therefore could be a non-optimal strategy (Lau et al., 2002). Therefore, before undertaking costly rehabilitation projects to reduce inflow infiltration, it is crucial to emphasize the need for a comprehensive analysis of malfunctions in ageing sewers (Su et al., 2020). Despite the effort represented by the reduction of infiltration inflow, it does not seem to be sufficient and should be supported by other actions.

Stormwater disconnection scenarios could have a higher efficiency for CSO mitigation. In the present study, simulations shown that almost half of the CSO volume could be suppressed by disconnecting the first 10 mm of rain on impervious surfaces. Montoya-Coronado et al. (2022) found similar results when modelling the same stormwater disconnection scenarios. Additionally, D'Ambrosio et al. (2022), Joshi et al. (2021) and Riechel et al. (2020) also obtained comparable findings when modelling stormwater disconnection scenarios with a more detailed description of the type and location of source-control devices. They found that disconnecting 20 % of impervious surfaces could result in a reduction from 30 to 75 % of the CSO volume.

5. Conclusion

A parsimonious model has been developed to evaluate and quantify the contribution of permanent infiltration inflow and rainfall-induced infiltration to CSO in a typical urban catchment. The present methodology shows how to identify and simulate the following flow components in the hydrograph observed at the catchment outlet: wastewater, impervious and permeable surface runoff, permanent infiltration inflow and rain-induced infiltration inflow. The observations of each flow component's behaviors guided the construction of a simplified model that could conceptually represent the surface, subsurface and sewer processes. To describe the fraction and dynamic of those flow components, nine parameters have been calibrated from data pretreatment.

The comparison between observed data and simulation showed the model's capacity to provide a satisfactory simulation of the hydrograph, notably most of the peak values and the depletion curves. However, some peaks were not well reproduced, which may result in large differences with the observed CSO volume. The error on the total CSO volume was acceptable for practical purposes, along with a good reproduction of the CSO frequency over long periods. Model application included the determination of the proportion of each flow component that reached the CSO structure. Results showed that, at annual scale, ~53 % of the outlet volume corresponds to wastewater, ~10 % to runoff water and ~37 % to sub-surface infiltrated water. The latter, which is expected to increase over the years due to pipe ageing, has been analyzed under permanent infiltration inflow and rain induced infiltration reduction scenarios. Eliminating infiltration inflow could represent between 11 and 17 % of annual CSO volume reduction. However, this strategy is of limited interest for reducing the CSO frequency and CSO duration. On the other hand, the implementation of source-control stormwater management strategies shows promising perspective that could complement rehabilitation scenarios. For example, by disconnecting the first 10 mm of rainfall, it is possible to completely eliminate the CSO volume for half of the CSO events.

The use of these assessment methods can support the decision-makers on the degree of effort required to reduce CSO volumes and frequency. Further work should extend the analysis to other study areas (by discretizing into sub-catchments), test the limitations of the approach, and integrate global change scenarios. Further research could consider additional sources of rainfall-induced infiltration (RII), such as the seasonal impact of the water table during rainy periods and potential rainwater infiltration from stormwater management source control infrastructures. Additionally, the growing frequency of extreme weather events resulting from climate change must not be disregarded, and the impact of RII on CSO should be investigated.

CRediT authorship contribution statement

V.A. Montoya-Coronado: Conceptualization, Formal analysis, Investigation, Methodology, Software, Validation, Visualization, Writing – original draft. **D. Tedoldi:** Conceptualization, Investigation, Methodology, Project administration, Supervision, Validation, Writing – review & editing. **H. Castebrunet:** Conceptualization, Funding acquisition, Methodology, Project administration, Supervision, Validation, Writing – review & editing. **P. Molle:** Funding acquisition, Methodology, Project administration, Supervision, Validation, Writing – review & editing. **G. Lipeme Kouyi:** Funding acquisition, Methodology, Project administration, Supervision, Validation, Writing – review & editing.

Declaration of competing interest

The authors declare that they have no known competing financial interests or personal relationships that could have appeared to influence the work reported in this paper.

Data availability

Data will be made available on request.

Acknowledgements

The authors would like to thank the Office Français de la Biodiversité, Rhône–Méditerranée–Corse and Adour-Garonne water agencies for their financial support to the TONIC research project. This work was carried out with the support of the EUR H2O'Lyon (ANR-17-EURE-0018) of the University of Lyon (UdL) as part of the "Investissements d'Avenir" program managed by the French National Research Agency (ANR) and performed in part within the framework of the OTHU (Field Observatory for Urban Water Management – http://othu.org) and the MULTISOURCE project, funded by the European Union's Horizon.

H2020-EU.3.5.2. under grant agreement 101003527.

Appendix A. Supplementary data

Supplementary data to this article can be found online at https://doi.org/10.1016/j.jhydrol.2024.130834.

References

Andrés-Doménech, I., Múnera, J.C., Francés, F., Marco, J.B., 2010. Coupling urban event-based and catchment continuous modelling for combined sewer overflow river impact assessment. Hydrol. Earth Syst. Sci. 14, 2057–2072. https://doi.org/10.5194/hess-14-2057-2010.

Armson, D., Stringer, P., Ennos, A.R., 2013. The effect of street trees and amenity grass on urban surface water runoff in Manchester, UK. Urban For. Urban Green. 12, 282–286. https://doi.org/10.1016/j.ufug.2013.04.001.

Arora, M., Malano, H., Davidson, B., Nelson, R., George, B., 2015. Interactions between centralized and decentralized water systems in urban context: a review. WIREs Water 2, 623–634. https://doi.org/10.1002/wat2.1099.

Asadian, Y., Weiler, M., 2009. A New Approach in Measuring Rainfall Interception by Urban Trees in Coastal British Columbia. Water Quality Research Journal 44, 16–25. https://doi.org/10.2166/wqrj.2009.003.

Bareš, V., Stránský, D., Sýkora, P., 2009. Sewer infiltration/inflow: long-term monitoring based on diurnal variation of pollutant mass flux. Water Sci. Technol. 60, 1–7. https://doi.org/10.2166/wst.2009.280.

Beheshti, M., 2015. Infiltration / Inflow Assessment and Detection in Urban Sewer System 12.

Bentes, I., Silva, D., Vieira, C., Matos, C., 2022. Inflow quantification in urban sewer networks. Hydrology 9, 52. https://doi.org/10.3390/hydrology9040052.

Bertrand-Krajewski, J.-L., Uhl, M., Clemens-Meyer, F.H.L.R., 2021. Uncertainty Assessment. https://doi.org/10.2166/9781789060119_0263.

Bonneau, J., Fletcher, T.D., Costelloe, J.F., Burns, M.J., 2017. Stormwater infiltration and the 'urban karst' – A review. J. Hydrol. 552, 141–150. https://doi.org/10.1016/j.jhydrol.2017.06.043.

Bonneau, J., Branger, F., Castebrunet, H., Lipeme Kouyi, G., 2023. The impact of stormwater management strategies on the flow regime of a peri-urban catchment facing urbanisation and climate change: a distributed modelling study in Lyon, France. Urban Water J. 1–18. https://doi.org/10.1080/1573062X.2023.2217809.

Botturi, A., Ozbayram, E.G., Tondera, K., Gilbert, N.I., Rouault, P., Caradot, N., Gutierrez, O., Daneshgar, S., Frison, N., Akyol, Ç., Foglia, A., Eusebi, A.L., Fatone, F., 2021. Combined sewer overflows: a critical review on best practice and innovative solutions to mitigate impacts on environment and human health. Crit. Rev. Environ. Sci. Technol. 51, 1585–1618. https://doi.org/10.1080/10643389.2020.1757957.

Boyd, M.J., Bufill, M.C., Knee, R.M., 1993. Pervious and impervious runoff in urban catchments. Hydrol. Sci. J. 38, 463–478. https://doi.org/10.1080/02626669309492699.

Chocat, B., 2013. In: CANOE: an Urban Hydrology Software Package. Modeling Software. John Wiley & Sons Inc, Hoboken, NJ USA, pp. 209–218. https://doi.org/10.1002/9781118557891.ch17.

D'Ambrosio, R., Balbo, A., Longobardi, A., Rizzo, A., 2022. Re-think urban drainage following a SuDS retrofitting approach against urban flooding: A modelling investigation for an Italian case study. Urban For. Urban Green. 70, 127518 https://doi.org/10.1016/j.ufug.2022.127518.

De Bénédittis, J., Bertrand-Krajewski, J.-L., 2005. Infiltration in sewer systems: comparison of measurement methods. Water Sci. Technol. 52, 219–227. https://doi.org/10.2166/wst.2005.0079.

Desbordes, M., 1974. Réflexions sur les méthodes de calcul des réseaux urbains d'assainissement pluvial. Université des Sciences et Techniques, Languedoc, Montpellier, France.

Desbordes, M., Ramperez, A., 1977. Extension du modèle L.H.M. aux bassins versants de taille moyenne. Université de Montpellier, France.

Dirckx, G., Fenu, A., Wambecq, T., Kroll, S., Weemaes, M., 2019. Dilution of sewage: Is it, after all, really worth the bother? J. Hydrol. 571, 437–447. https://doi.org/10.1016/j.jhydrol.2019.01.065.

Ellis, B., Bertrand-Krajewski, J.-L., 2010. Assessing Infiltration and Exfiltration on the Performance of Urban Sewer Systems. IWA Publishing.

Fletcher, T.D., Andrieu, H., Hamel, P., 2013. Understanding, management and modelling of urban hydrology and its consequences for receiving waters: a state of the art. Adv. Water Resour. 51, 261–279. https://doi.org/10.1016/j.advwatres.2012.09.001.

Fryd, O., Backhaus, A., Birch, H., Fratini, C.F., Ingvertsen, S.T., Jeppesen, J., Panduro, T. E., Roldin, M., Jensen, M.B., 2013. Water sensitive urban design retrofits in Copenhagen – 40% to the sewer, 60% to the city. Water Sci. Technol. 67, 1945–1952. https://doi.org/10.2166/wst.2013.073.

Golden, H.E., Hoghooghi, N., 2018. Green infrastructure and its catchment-scale effects: an emerging science. WIREs Water 5. https://doi.org/10.1002/wat2.1254.

Gupta, H.V., Kling, H., Yilmaz, K.K., Martinez, G.F., 2009. Decomposition of the mean squared error and NSE performance criteria: Implications for improving hydrological modelling. J. Hydrol. 377, 80–91. https://doi.org/10.1016/j.jhydrol.2009.08.003.

Harbaugh, A.W., 2005. MODFLOW-2005, the US Geological Survey modular ground-water model: the ground-water flow process. US Department of the Interior, US Geological Survey Reston, VA, USA.

Hernes, R.R., Gragne, A.S., Abdalla, E.M.H., Braskerud, B.C., Alfredsen, K., Muthanna, T. M., 2020. Assessing the effects of four SUDS scenarios on combined sewer overflows in Oslo, Norway: evaluating the low-impact development module of the Mike Urban model. Hydrology Research 51, 1437–1454. https://doi.org/10.2166/nh.2020.070.

Jean, M.-È., Morin, C., Duchesne, S., Pelletier, G., Pleau, M., 2021. Optimization of real-time control with green and gray infrastructure design for a cost-effective mitigation of combined sewer overflows. Water Resour. Res. 57, e2021WR030282 https://doi.org/10.1029/2021WR030282.

Jean, M., Morin, C., Duchesne, S., Pelletier, G., Pleau, M., 2022. Real-time model predictive and rule-based control with green infrastructures to reduce combined sewer overflows. Water Res. 221, 118753 https://doi.org/10.1016/j.watres.2022.118753.

Joshi, P., Leitão, J.P., Maurer, M., Bach, P.M., 2021. Not all SuDS are created equal: Impact of different approaches on combined sewer overflows. Water Res. 191, 116780 https://doi.org/10.1016/j.watres.2020.116780.

Kidd, C.H.R., 1978. Rainfall-runoff processes over urban surfaces. Proceedings of an International Workshop Held at IH, April 1978 [WWW Document] accessed 3.24.23.

Kidmose, J., Troldborg, L., Refsgaard, J.C., Bischoff, N., 2015. Coupling of a distributed hydrological model with an urban storm water model for impact analysis of forced infiltration. J. Hydrol. 525, 506–520. https://doi.org/10.1016/j.jhydrol.2015.04.007.

Kouchi, D.H., Esmaili, K., Faridhosseini, A., Sanaeinejad, S.H., Khalili, D., Abbaspour, K. C., 2017. Sensitivity of calibrated parameters and water resource estimates on different objective functions and optimization algorithms. Water 9, 384. https://doi.org/10.3390/w9060384.

Kracht, O., Gujer, W., 2005. Quantification of infiltration into sewers based on time series of pollutant loads. Water Sci. Technol. 52, 209–218. https://doi.org/10.2166/wst.2005.0078.

Lau, J., Butler, D., Schütze, M., 2002. Is combined sewer overflow spill frequency/volume a good indicator of receiving water quality impact? Urban Water 4, 181–189. https://doi.org/10.1016/S1462-0758(02)00013-4.

Leopold, L.B., 1991. Lag times for small drainage basins. Catena 18, 157–171. https://doi.org/10.1016/0341-8162(91)90014-O.

Libralato, G., Volpi Ghirardini, A., Avezzù, F., 2012. To centralise or to decentralise: An overview of the most recent trends in wastewater treatment management. J. Environ. Manage. 94, 61–68. https://doi.org/10.1016/j.jenvman.2011.07.010.

Liu, T., Ramirez-Marquez, J.E., Jagupilla, S.C., Prigiobbe, V., 2021. Combining a statistical model with machine 633 learning to predict groundwater flooding (or infiltration) into sewer networks. Journal of Hydrology 603, 634–126916. https://doi.org/10.1016/j.jhydrol.2021.126916.

Mahaut, V., Andrieu, H., 2019. Relative influence of urban-development strategies and water management on mixed (separated and combined) sewer overflows in the context of climate change and population growth: a case study in Nantes. Sustain. Cities Soc. 44, 171–182. https://doi.org/10.1016/j.scs.2018.09.012.

Marsalek, J., Chocat, B., 2002. International Report: Stormwater management. Water Sci. Technol. 46, 1–17. https://doi.org/10.2166/wst.2002.0657.

Momplot, A., 2014. Modélisation tridimensionnelle des écoulements en réseau d'assainissement : Evaluation des modèles RANS à travers l'étude des écoulements au droit d'ouvrages spéciaux (These de doctorat). INSA, Lyon.

Montoya-Coronado, V.A., Bret, P., Molle, P., Castebrunet, H., Tedoldi, D., Lipeme Kouyi, G., 2022. Stratégies de déconnexion des eaux pluviales à l'échelle d'un bassin versant pour réduire les déversements: C. TSM 27–37. https://doi.org/10.36904/tsm/202204027.

Pangle, L.A., Diem, J.E., Milligan, R., Adams, E., Murray, A., 2022. Contextualizing inflow and infiltration within the streamflow regime of urban watersheds. Water Resour. Res. 58, e2021WR030406 https://doi.org/10.1029/2021WR030406.

Pophillat, W., Sage, J., Rodriguez, F., Braud, I., 2021. Dealing with shallow groundwater contexts for the modelling of urban hydrology – a simplified approach to represent interactions between surface hydrology, groundwater and underground structures in hydrological models. Environ. Model. Softw. 144, 105144 https://doi.org/10.1016/j.envsoft.2021.105144.

Ragab, R., Rosier, P., Dixon, A., Bromley, J., Cooper, J.D., 2003. Experimental study of water fluxes in a residential area: 2. road infiltration, runoff and evaporation. Hydrol. Process. 17, 2423–2437. https://doi.org/10.1002/hyp.1251.

Ramier, D., Berthier, E., Andrieu, H., 2011. The hydrological behaviour of urban streets: long-term observations and modelling of runoff losses and rainfall–runoff transformation. Hydrol. Process. 25, 2161–2178. https://doi.org/10.1002/hyp.7968.

Rammal, M., Berthier, E., 2020. Runoff losses on urban surfaces during frequent rainfall events: a review of observations and modeling attempts. Water 12, 2777. https://doi.org/10.3390/w12102777.

Rao, R.A., Delleur, J.W., 1974. Instantaneous unit hydrographs, peak discharges and time lags in urban basins. Hydrol. Sci. Bull. 19, 185–198. https://doi.org/10.1080/02626667409493898.

Riechel, M., Matzinger, A., Pallasch, M., Joswig, K., Pawlowsky-Reusing, E., Hinkelmann, R., Rouault, P., 2020. Sustainable urban drainage systems in established city developments: modelling the potential for CSO reduction and river impact mitigation. J. Environ. Manage. 274, 111207 https://doi.org/10.1016/j.jenvman.2020.111207.

Roldin, M., Fryd, O., Jeppesen, J., Mark, O., Binning, P.J., Mikkelsen, P.S., Jensen, M.B., 2012. Modelling the impact of soakaway retrofits on combined sewage overflows in a 3km2 urban catchment in Copenhagen, Denmark. J. Hydrol. 452–453, 64–75. https://doi.org/10.1016/j.jhydrol.2012.05.027.

Salvadore, E., Bronders, J., Batelaan, O., 2015. Hydrological modelling of urbanized catchments: a review and future directions. J. Hydrol. 529, 62–81. https://doi.org/10.1016/j.jhydrol.2015.06.028.

Schulz, N., Baur, R., Krebs, P., 2005. Integrated modelling for the evaluation of infiltration effects. Water Sci. Technol. 52, 215–223. https://doi.org/10.2166/wst.2005.0136.

Sitzenfrei, R., Möderl, M., Rauch, W., 2013. Assessing the impact of transitions from centralised to decentralised water solutions on existing infrastructures – integrated city-scale analysis with VIBe. Water Res. 47, 7251–7263. https://doi.org/10.1016/j.watres.2013.10.038.

Staufer, P., Scheidegger, A., Rieckermann, J., 2012. Assessing the performance of sewer rehabilitation on the reduction of infiltration and inflow. Water Res. 46, 5185–5196. https://doi.org/10.1016/j.watres.2012.07.001.

Sowby, R.B., Jones, D.R., 2022. A Practical Statistical Method to Differentiate Inflow and Infiltration in Sanitary 665 Sewer Systems. Journal of Environmental Engineering 148, 06021006. 666 https://doi.org/10.1061/(ASCE)EE.1943-7870.0001962.

Su, X., Liu, T., Beheshti, M., Prigiobbe, V., 2020. Relationship between infiltration, sewer rehabilitation, and groundwater flooding in coastal urban areas. Environ Sci Pollut Res 27, 14288–14298. https://doi.org/10.1007/s11356-019-06513-z.

The European Federation of National Water Services, 2017. Europe's water in figures : An overview of the European drinking water and waste water sectors.

Torres, M.N., Rabideau, A., Ghodsi, S.H., Zhu, Z., Shawn Matott, L., 2022. Spatial design strategies and performance of porous pavements for reducing combined sewer overflows. J. Hydrol. 607, 127465 https://doi.org/10.1016/j.jhydrol.2022.127465.

Wang, S., Wang, H., 2018. Extending the Rational Method for assessing and developing sustainable urban drainage systems. Water Res. 144, 112–125. https://doi.org/10.1016/j.watres.2018.07.022.

Wang, M., Zhang, M., Shi, H., Huang, X., Liu, Y., 2019. Uncertainty analysis of a pollutant-hydrograph model in assessing inflow and infiltration of sanitary sewer systems. J. Hydrol. 574, 64–74. https://doi.org/10.1016/j.jhydrol.2019.04.011.

Weiß, G., Brombach, H., Haller, B., 2002. Infiltration and inflow in combined sewer systems: long-term analysis. Water Sci. Technol. 45, 11–19. https://doi.org/10.2166/wst.2002.0112.

Zhang, M., Liu, Y., Cheng, X., Zhu, D.Z., Shi, H., Yuan, Z., 2018. Quantifying rainfall-derived inflow and infiltration in sanitary sewer systems based on conductivity monitoring. J. Hydrol. 558, 174–183. https://doi.org/10.1016/j.jhydrol.2018.01.002.

Zhang, K., Parolari, A.J., 2022. Impact of stormwater infiltration on rainfall-derived inflow and infiltration: a physically based surface–subsurface urban hydrologic model. J. Hydrol. 610, 127938 https://doi.org/10.1016/j.jhydrol.2022.127938.

Zhou, Q., 2014. A Review of Sustainable Urban Drainage Systems Considering the Climate Change and Urbanization Impacts. Water 6, 976–992. https://doi.org/10.3390/w6040976.

Zhou, Q., Leng, G., Su, J., Ren, Y., 2019. Comparison of urbanization and climate change impacts on urban flood volumes: Importance of urban planning and drainage adaptation. Sci. Total Environ. 658, 24–33. https://doi.org/10.1016/j.scitotenv.2018.12.184.